Multiple instabilities in $Bi_4Ti_3O_{12}$: A ferroelectric beyond the soft-mode paradigm

J. M. Perez-Mato,[1,*] P. Blaha,[2] K. Schwarz,[2] M. Aroyo,[1] D. Orobengoa,[1] I. Etxebarria,[3] and Alberto García[4]
[1]*Departamento de Física de la Materia Condensada, Facultad de Ciencia y Tecnología, Universidad del País Vasco, Apartado 644, E-48080 Bilbao, Spain*
[2]*Institute of Materials Chemistry, Vienna University of Technology, A-1060 Vienna, Getreidemarkt 9/165-TC, Austria*
[3]*Fisika Aplikatua II Saila, Zientzia eta Teknologia Facultatea, Euskal Herriko Unibertsitatea, P.K. 644, E-48080 Bilbao, Spain*
[4]*Institut de Ciencia de Materials de Barcelona, CSIC, Campus de la UAB, E-08193 Bellaterra, Spain*
(Received 25 February 2008; published 7 May 2008)

The Aurivillius compound $Bi_4Ti_3O_{12}$ exhibits a single phase transition from a tetragonal high-temperature phase to a ferroelectric state. By means of first-principles calculations guided by a complete symmetry analysis of the experimental distortion, we confirm $B1a1$ as the (monoclinic) symmetry of the room-temperature phase but show that the transition involves a complex interplay of six different normal modes belonging to four different irreducible representations. Three of them are necessary for the observed symmetry break. We do not find any feature in the energy landscape that would force the simultaneous condensation of these three order parameters and cause such an avalanche transition, so we suggest that further experimental work might be able to detect intermediate phases. On the other hand, the necessary condensation of pairs of normal modes of the same symmetry already puts $Bi_4Ti_3O_{12}$ outside the standard soft-mode paradigm and has important structural implications. In particular, the approximate rigidity of the BiO_6 octahedra is due to anharmonic couplings of these modes. In addition, a comparison of the energy calculations and the behavior of the bond-valence global instability index is presented.

DOI: 10.1103/PhysRevB.77.184104 PACS number(s): 77.80.Bh, 61.50.Ks, 63.20.dk, 64.70.K−

I. INTRODUCTION

A renewed interest in the theoretical study and design of ferroelectric materials has arisen in recent years. One of the reasons for this upsurge of activity has been the new possibilities which *ab initio* density functional theory (DFT) calculations have opened. For the simple perovskites such as $BaTiO_3$ or $PbTiO_3$, numerous DFT calculations (see Refs. 1–3 for some reviews) have clearly demonstrated that the thermal transition mechanism leading to the ferroelectric phase(s) can be described by what we can call the "unstable-mode" model, which can be summarized by the following features:

(1) At 0 K, the paraelectric high-symmetry phase is unstable with respect to a polar optic mode at the Brillouin zone center. Although other unstable modes may exist, this (in general degenerate) polar mode is clearly the strongest instability of the paraelectric cubic structure, with the largest imaginary frequency.

(2) The phonon branch of the unstable polar mode is basically the only unstable phonon branch. If some other soft branches exist, they are clearly separated from the polar mode and have much smaller imaginary frequencies.

(3) In the ferroelectric phase, the experimental structural distortion agrees well with the calculated unstable mode.

(4) The calculated (quartic) anharmonicity of the modes of the whole unstable polar phonon branch is approximately constant, which implies that it has a local character.

These properties allow an approximate description of the behavior of these systems by considering as active degrees of freedom only the modes of the unstable soft-mode phonon branch, while the remaining modes can be subsumed in the heat bath. The corresponding effective Hamiltonian is then a sort of generalized ϕ^4 model[4] with a single vectorlike local degree of freedom per unit cell, and the anharmonic terms are Einstein-like, i.e., a crystal field on the local variable.

The formalism based on this type of effective Hamiltonian, with parameters calculated by first-principles methods, has been very successful in reproducing and predicting the essential properties of not only pure ferroelectric perovskites but also those of compounds with mixed compositions such as $Pb[Zr,Ti]O_3$ (PZT) (see Refs. 1–3 and references therein).

More complicated situations can happen when several modes that correspond to quite different local degrees of freedom are unstable. For instance, in $SrTiO_3$, an instability at the border of the Brillouin zone, corresponding to a rigid-unit mode (RUM) of the octahedra, is stronger than the ferroelectric one and prevails over it.[5] This is one of the simplest examples of competition among structural instabilities.

The situation is even more complex in the Aurivillius compounds, which exhibit a higher number of competing structural instabilities. These compounds are layered bismuth oxides formed by stacking Bi_2O_2 slabs and perovskitelike blocks. Their high-temperature phase has $I4/mmm$ symmetry. Many of them are ferroelectric at room temperature, but in addition to the polar distortion, they have other nonpolar antiferrodistortive distortions, which involve large tiltings of the perovskitelike octahedra.[6–9] For one specific member of the family, namely, $SrBi_2Ta_2O_9$ (SBT), by means of *ab initio* calculations combined with a structural and symmetry analysis, we have demonstrated that a complex interplay exists between three structural instabilities including the ferroelectric one.[10] This situation is expected to be common for the whole family, since the symmetry of the ferroelectric phases in all these compounds cannot be explained by considering only the symmetry break due to the ferroelectric distortion. At least the spontaneous freezing of one of the other unstable modes is necessary in order to explain the observed symme-

try. This requirement characterizes these systems, so that they are beyond the simple single unstable-mode model summarized above.

According to the basic paradigm of the Landau theory of structural phase transitions,[11,12] in SBT, one expects the existence of two phase transitions, one for each of the two symmetry-breaking modes that can explain the final symmetry of the room-temperature ferroelectric phase, and, indeed, this is what has recently been observed in this compound.[13–15] However, such sequence of two phase transitions seems to be absent in other analogous members of the family, such as $SrBi_2NbO_9$ (SBN) and $Bi_5Ti_3FeO_{15}$,[16] for which the two modes seem to condense simultaneously. This situation is quite peculiar, since, in general, it is not expected that more than one symmetry-breaking mode is active at a single transition. For second order transitions, this would only happen by pure coincidence, whereas in first-order transitions, the simultaneous freezing of two independent modes is a rare phenomenon, which is usually attributed to a so-called triggering mechanism, requiring a (negative) coupling that strongly favors the simultaneous presence of the two modes.[12,17,18] This type of coupling is very rare, as it usually has the opposite sign, i.e., the freezing of a single mode positively renormalizes (i.e., stabilizes) through an anharmonic coupling the other unstable modes (for instance, those of the corresponding phonon branch). This explains why transition order parameters of first order or discontinuous structural phase transitions can, in general, also be associated with a single irreducible representation (irrep) of the high-symmetry space group, i.e., with a single mode instability. In the following, we shall call *avalanche* transitions those that break this basic rule of Landau's theory, i.e., those in which several irreps (order parameters) are required to explain the symmetry break taking place. This term does not prejudge the possible mechanism responsible for this type of behavior.

In Ref. 10, we were able to show that in SBT, the biquadratic couplings between the three dominant unstable modes had the usual positive sign which precludes a triggering mechanism. Furthermore, the allowed trilinear coupling of the three unstable modes was too small to act as an alternative triggering mechanism. Therefore, two consecutive transitions were predicted, in agreement with experiment. However, as stressed above, in some other Aurivillius compounds, such as SBN, no intermediate phase has been detected, despite being isomorphous with SBT in both the high and the room-temperature phase.

$Bi_4Ti_3O_{12}$ (BTO) apparently has also a single avalanche transition at 670 °C between its tetragonal high-temperature phase and its ferroelectric room-temperature phase. While SBT and SBN have a thickness of two perovskite slabs with BO_6 octahedra, in the case of BTO, the perovskite slabs are three-octahedra thick (see Fig. 1). The ferroelectric phase of BTO has been reported to be monoclinic, and its symmetry would require at least the condensation of three different symmetry-breaking modes corresponding to three different irreps. Although a claim of the presence of an intermediate phase[19] has been published, it has not been confirmed and a single phase transition between the tetragonal and the ferroelectric phase has been reported in multiple studies and is commonly accepted.[12] Here, we perform *ab initio* total-energy and phonon calculations to determine the features that distinguish BTO from SBT, in relation to this conspicuous behavior. We analyze our results within a group theoretical framework that allows us to make a thorough quantitative comparison with experimental structural results and to extract physical insight into the interplay of the different mechanisms involved in the ferroelectric phase of this compound, in particular, the possibility of a triggering mechanism for the avalanche transition.[38]

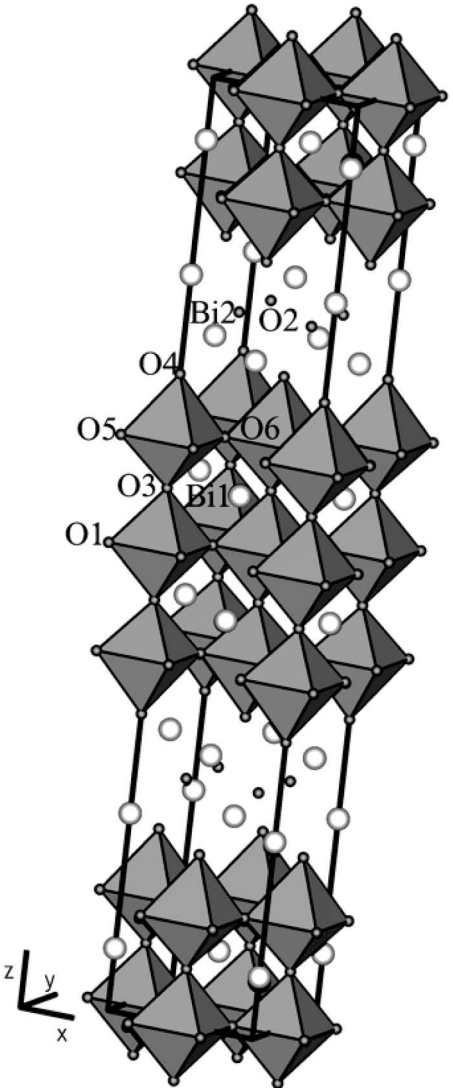

FIG. 1. Structure of $Bi_4Ti_3O_{12}$ in the high-temperature tetragonal phase with space group $I4/mmm$.

A first-principles study of $Bi_4Ti_3O_{12}$ was reported in Ref. 20, but only the polar instability was analyzed and the other distorting modes present in the ferroelectric phase that are necessary to explain the observed structure were not considered.

II. COMPUTATIONAL DETAILS

The details of the *ab initio* calculations presented here are the following. We used the linearized augmented plane

wave+local orbitals code WIEN2K.[21] Exchange and correlation were treated within the generalized gradient approximation (GGA) by using the Perdew-Burke-Ernzerhof (PBE) parametrization.[22] The atomic sphere radii R_{mt} were chosen as 2.28, 1.74, and 1.54 bohr for Bi, Ti, and O, respectively. The parameter $R_{mt}K_{max}$ determining the plane wave basis set was 6.5 for all calculations. Depending on the size of the unit cell or supercell used, the k mesh was varied, but typically, we used $4\times4\times4$ shifted Monkhorst–Pack meshes in the smaller unit cells and equivalent meshes for larger cells.

The phonon spectrum of the system was computed by first performing WIEN2K force calculations for selected symmetry-adapted distortions that were determined with the help of the PHONON package,[23] starting from a fully relaxed tetragonal structure in a 76-atom supercell. Then, the so-called direct method implemented in PHONON (Ref. 23) was used. Effective atomic force constants were obtained from the forces of 40 selected configurations and triclinic symmetry. In each of the first 20 configurations, a single atom was displaced by +0.05 Å in the x, y, or z direction, while the other 20 involved the opposite displacements. Pairs of calculations with positive and negative displacements were combined to get rid of quadratic response effects and minimize errors. From these force constants, the dynamical matrix for many q vectors was generated to compute the phonon branches. Phonon calculations require highly accurate forces, so we chose for the forces a rather strict self-consistency convergence criterion, typically 0.1 mRy/bohr. For the more relevant symmetries, static normal modes and their stiffness were recalculated by frozen phonon calculations restricted to the required symmetry-adapted subspaces.

In addition to the first-principles analysis, we have carried out some calculations within the bond-valence model to check whether the approximate mapping we found in Ref. 24 for the low-lying modes of SBT is maintained for $Bi_4Ti_3O_{12}$. These calculations are presented in the Appendix.

III. MONOCLINIC GROUND STATE

An initial fundamental problem in BTO concerns the actual symmetry and structure of the room-temperature phase. While numerous powder x-ray and neutron powder diffraction studies, including very recent ones,[19,25] reported a structure with space group $B2cb$ (No. 41) (keeping the setting of the tetragonal phase),[39] a single-crystal x-ray analysis[7] claimed that the phase is monoclinic, with space group $B1a1$. Within experimental resolution, this monoclinic structure would keep an orthogonal unit cell. Monoclinic features were also reported by macroscopic measurements.[26] In order to elucidate this first controversy on the symmetry of the compound, we performed DFT calculations and relaxed the structure of BTO under the $B1a1$ symmetry keeping the lattice parameters fixed to the experimental values. This symmetry includes the alternative orthorhombic space group $B2cb$ as a supergroup.

To compare the final relaxed structure with the experimental one, it is convenient to describe both in terms of symmetry-adapted distortions. In complex cases as this one, in which several modes of different symmetries may be frozen, the number of variant (twinned) equivalent structures is very large, involving correlated sign changes of some of the intervening frozen modes. This precludes, in general, a direct comparison of the structures. In the present case, the space of distortions with $B1a1$ symmetry has seven subspaces that can be distinguished by different irreps of $I4/mmm$ or, as pointed out in Ref. 7, by the different space groups that they keep invariant. These can be readily obtained by using the tools present in the Bilbao Crystallographic Server (www.cryst.ehu.es).[28,29] The subspaces are X_3^+ ($Bmab$, No. 64), E_u ($F2mm$, No. 42), X_1^- ($Bbab$, No. 68), X_2^+ ($Bbam$, No. 64), E_g ($I12/m1$, No. 12), A_u ($I4mm$, No. 107), and X_4^- ($Bmam$, No. 67), where two-dimensional irreps should be restricted to the necessary subspace. The invariance space group (in a common nonstandard setting) is indicated in parenthesis together with its number in the International Tables of Crystallography[27] (see Fig. 2).

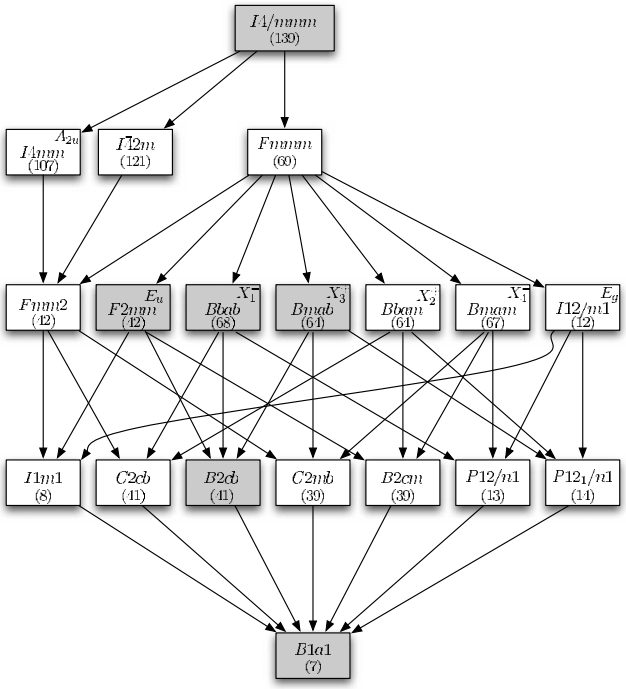

FIG. 2. Group-subgroup graph connecting the space groups $I4/mmm$ and $B1a1$. All intermediate subgroups are indicated. If existing, the irreducible representation of $I4/mmm$ associated with symmetry-breaking modes yielding the given intermediate symmetry is also given. The symmetries associated with the dominant orthorhombic distortion in BTO are highlighted.

The polar E_u distortion is responsible for the spontaneous polarization along the x axis, while the polar A_u mode would, in general, induce a polarization component along the z axis. The first three modes are compatible with the $B2cb$ space group, and the presence of two of them is sufficient for reducing the system to this symmetry, while any of the remaining four modes would further reduce the symmetry to $B1a1$. A $B1a1$ distortion has 51 additional degrees of freedom with respect to the $I4/mmm$ configuration, distributed into seven subspaces with dimensions (8, 11, 3, 5, 8, 9, 7), following the order indicated above. This means, for instance, that the experimental distortion of symmetry X_3^+ can be described by a

TABLE I. Comparison between the experimental $B1a1$ structure of $Bi_4Ti_3O_{12}$ (Ref. 7) and the calculated relaxed structure under this space group. The amplitudes in bohr of the different symmetry-adapted distortion modes for the two structures are given in the first two rows. The third row lists the scalar product of the normalized polarization vectors for each mode corresponding to the experimental and the *ab initio* relaxed structures. Normalization has been done with respect to the tetragonal high-temperature unit cell. The first three columns correspond to the distortions compatible with the higher symmetry $B2cb$ under discussion.

	X_3^+	E_u	X_1^-	X_2^+	E_g	A_u	X_4^-
Experimental	1.60	1.43	0.96	0.62	0.08	0.22	0.13
Ab initio relaxed	−1.77	−1.33	1.07	0.82	−0.10	0.25	−0.11
Scalar product	0.998	0.996	0.998	0.99	0.73	0.80	0.64

normalized eight-dimensional "polarization vector" plus a global amplitude $Q_{X_3^+}$ with dimensions of length. By decomposing the experimental $B1a1$ structure[7] in this form,[40] we obtain the amplitudes (in bohr) for the seven different symmetry-breaking distortion modes, listed in Table I. The polarization vectors were normalized within a single primitive unit cell of the reference tetragonal structure. Although the polarization vectors of the distortion modes with different symmetries can be very different, it is important to note that their amplitudes are expressed in a common absolute scale and thus can be compared, yielding their relative weights. The numbers in Table I immediately indicate the importance of the first two distortion modes in the $B2cb$ distortion, while it is clear that the X_2^+ distortion is the dominant one in the further break into $B1a1$ symmetry. The two strongest distortions, X_3^+ and E_u, are analogous to those present in SBT. X_3^+ involves a nearly rigid tilting around the x axis of the octahedra within the perovskite slabs, together with correlated displacements of the Bi atoms. This mode is responsible for the duplication of the unit cell. E_u is a polar mode that can be approximately described as a relative displacement along the x axis of the sublattice of Bi cations with respect to the slabs of TiO_6 octahedra. This mode is the cause of the spontaneous polarization along the x axis, and so the main responsible for the ferroelectric properties of the room-temperature phase. A second smaller component of the spontaneous polarization along z is caused by the A_u distortion mode.

Table I also shows the computed relaxed structure expressed in the same form. Apart from the amplitudes of the seven distortion modes, the table lists the projections of the associated polarization vectors on the corresponding ones of the experimental structure, as given by their scalar products. It can be seen that the agreement of the polarization vectors, which describe the internal structure of each symmetry-adapted distortion, is excellent for the dominant modes. The amplitudes of the seven distortion modes also agree very well but are, in general, systematically a bit larger for the *ab initio* structure. This is reasonable considering that the experimental structure was measured at room temperature and is being compared to a theoretical structure at 0 K. Order parameter amplitudes are not expected to have reached saturation at room temperature. It is important to note that some of the amplitudes have the opposite sign. This indicates that the calculation has arrived during the relaxation to a structure that is related to the experimental one by twinning and shows that, in general, a direct comparison of atomic coordinates between theoretical and experimental atomic positions would make no sense, as different modes with opposite amplitudes participate in the variation of some of the atomic coordinates. The twinning transformation relating the relaxed and the experimental structure is one of the eight possible ones for the symmetry breaking $I4/mmm \rightarrow B1a1$, disregarding those that imply a 90° rotation.

The excellent agreement between the experimental and theoretical monoclinic structures, especially with respect to the large distortion of X_2^+ symmetry, which breaks the orthorhombic symmetry of the other three dominant modes, confirms that $B1a1$, and not $B2cb$, must be the symmetry of the final distorted phase. This additional symmetry-breaking distortion only involves the rotations along the z axis of the central octahedra within the perovskite-type slabs. In this basic distortion, only a small number of oxygen atoms are involved and so this mode would produce minor changes in the diffraction diagram. This explains the difficulty in resolving the monoclinic distortion with powder diffraction techniques, since the unit cell is kept orthogonal within experimental resolution.

IV. NORMAL-MODE ANALYSIS OF THE TETRAGONAL PHASE: MULTIPLE UNSTABLE HARMONIC NORMAL MODES

From a direct generalization of the unstable-mode picture of the Introduction, one would expect that the experimental distortion in BTO should be the result of the freezing of unstable normal modes of the tetragonal structure whose symmetries and polarization vectors match those of the most significant distortions observed. There should then be one unstable X_3^+ and one unstable E_u normal modes, leading to a $B2cb$ distortion (with the E_u mode being responsible for the spontaneous polarization), and an X_2^+ normal mode, which is responsible for the final $B1a1$ symmetry through an additional significant distortion. The rest of the distorting modes of different symmetries present in the actual structure would be secondary, induced distortions compatible with the symmetry of the final configuration.

The relation of the static low-temperature structure of BTO with the harmonic normal modes of the high-temperature structure is actually much more complex. The calculation of the static normal modes of the $I4/mmm$ phase finds, indeed, that the two most unstable modes of the system have E_u and X_3^+ symmetries. In contrast to SBT, the polar mode E_u is much more unstable than the antiferrodistortive tilting mode (the modulus of its negative stiffness is significantly larger, and the depth of the associated energy well is about 30 mRy/f.u., compared to 15 mRy for the X_3^+ mode). However, there are multiple unstable "phonon" branches all along the Brillouin zone. These branches, as in SBT, can be traced back to a rough approximate "folding" of the branches of an ideal perovskite. The crucial point is that among these additional unstable branches, a second unstable mode of the

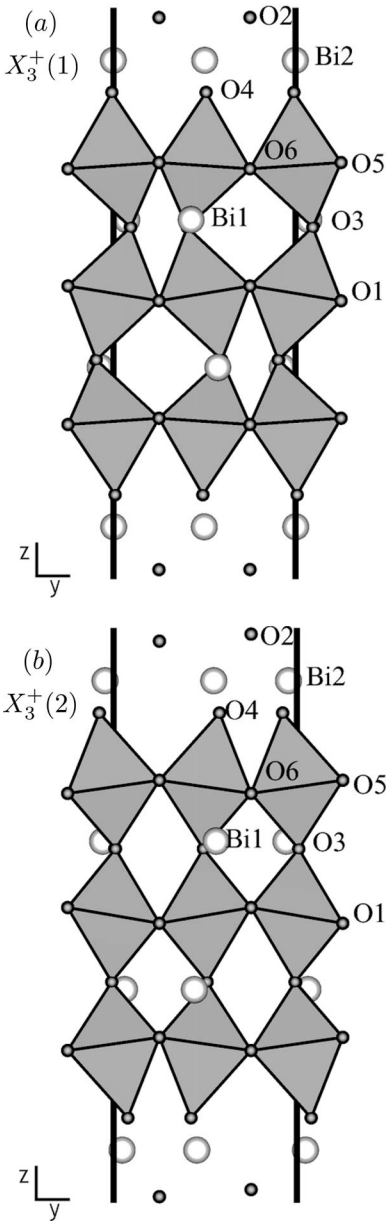

FIG. 3. (a) Projection along the x axis of the distortion produced by the most unstable X_3^+ normal mode [mode$X_3^+(1)$]. (b) The same for the second unstable X_3^+ normal mode [mode$X_3^+(2)$]. Mode amplitudes have been exaggerated (about 2 bohr) to stress the mode effects.

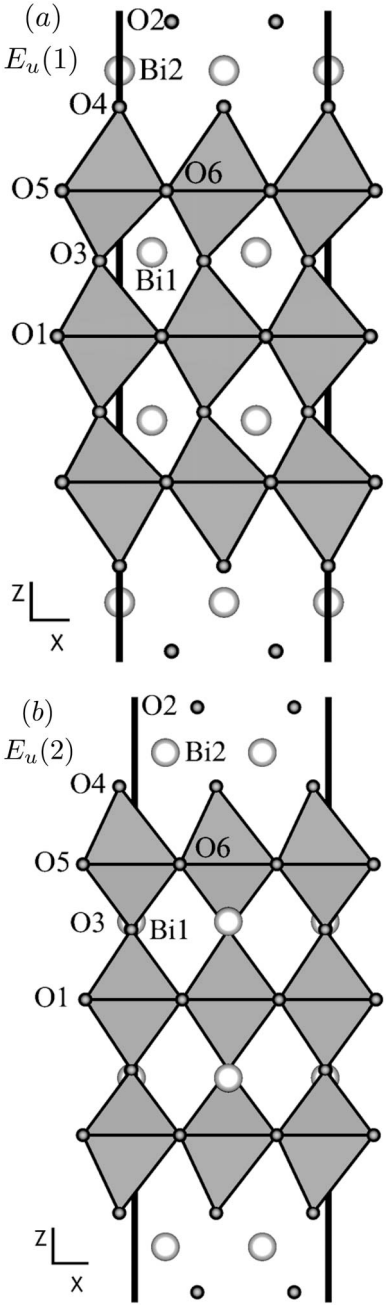

FIG. 4. (a) Projection along the y axis of the distortion produced by the most unstable E_u normal mode (mode $E_u(1)$). (b) The same for the second unstable E_u normal mode [mode $E_u(2)$]. Mode amplitudes have been exaggerated (about 3 bohr) to stress the mode effects.

relevant symmetries E_u and X_3^+ exists.[30] The distortions corresponding to these four unstable modes are depicted in Figs. 3 and 4, while the energy variation as a function of their amplitudes can be seen in Fig. 5. The most unstable X_3^+ mode [mode $X_3^+(1)$] is rather localized at the center of the perovskitelike slabs, tilting the central octahedra around the x axis but keeping the Bi_2O_2 layers and the apical oxygens of the neighboring octahedra essentially unchanged. This is in contrast to the second unstable X_3^+ mode [mode $X_3^+(2)$], which mainly involves displacements of the bismuth atoms in the Bi_2O_2 layers and also of the neighboring apical oxygens. It can be clearly seen that these two harmonic normal "soft" modes would strongly distort the BiO_6 octahedra if taken separately. Similarly, the most unstable E_u normal mode [mode $E_u(1)$] is localized at the center of the perovskite slabs and involves opposite displacements along x of the Bi and corresponding oxygens, while the second unstable one [mode $E_u(2)$], with a much weaker instability, involves a relative displacement of the Bi_2O_2 layers with respect to the apical oxygens in the neighboring octahedra (see Fig. 4).

As in the case of the X_3^+ modes, each E_u unstable normal mode produces, when considered in isolation, a considerable distortion of the octahedra in the perovskite slabs.

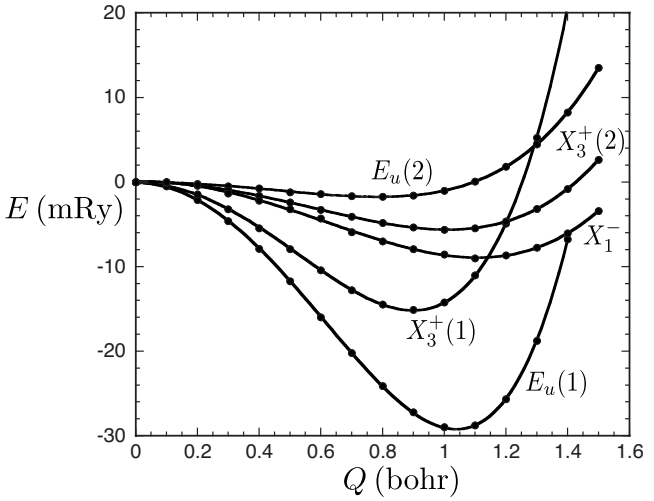

FIG. 5. Calculated energies per f.u. (relative to the tetragonal relaxed configuration) as a function of the amplitude of unstable static normal modes. The curves correspond to fitted 2-4-6 polynomials.

All this makes the energy landscape of BTO strikingly different from the one observed in SBT. In BTO, the low-energy dynamics in the harmonic approximation is far from respecting the assumed rigidity of the TiO_6 octahedra. On the contrary, as suggested in Ref. 31, it seems to be more in accordance with a monatomic layered picture of the Aurivillius compounds, with the normal modes combining layer displacements that do not necessarily keep the octahedra undistorted. Although the splitting and z localization of the normal modes are obtained at 0 K, one expects that it is maintained at high temperatures, at which the corresponding frequencies are normalized to real values, thus making the tetragonal phase stable. This would mean that in the tetragonal phase, contrary to what is commonly assumed, the TiO_6 octahedra have distorting normal modes with very low frequency. As one would expect from the localization with the eigenvectors of these modes, the corresponding calculated phonon branches are very flat along the z direction. This suggests a relaxational character for these modes and order-disorder behavior for the transition(s) where these modes are active, in agreement with recent experimental reports.[32] As in SBT, a normal mode with the third symmetry present in the dominant orthorhombic $B2cb$ distortion (X_1^- in this case) is also unstable. Its polarization vector agrees with that of the actual experimental distortion mode, and its instability is stronger than in SBT when compared with the main unstable normal modes (see Fig. 5).

V. NORMAL-MODE DECOMPOSITION OF THE EXPERIMENTAL STRUCTURE

Although the two additional unstable modes of symmetries X_3^+ and E_u produce only a much smaller decrease in the energy than the most unstable ones (see Figs. 5 and 6), they are present with nearly equal weight in the experimental static distortion. More specifically, the polarization vector describing the experimental X_3^+ distortion can be expressed in

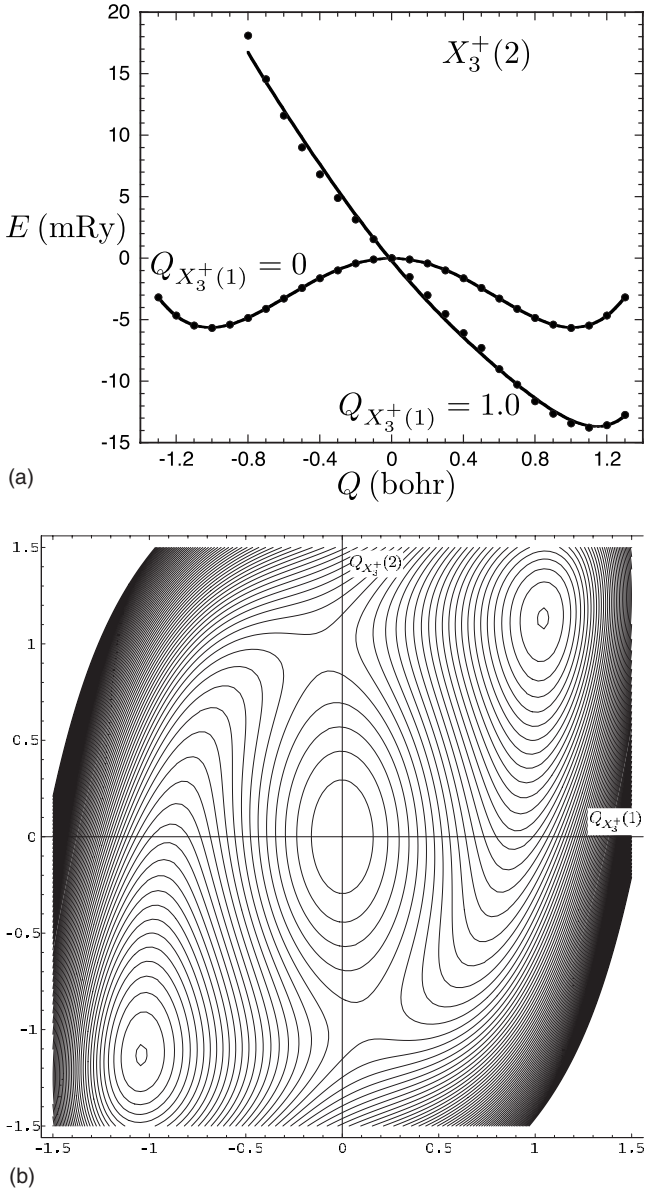

FIG. 6. (a) Relative change of the energy per f.u. as a function of the amplitude of mode $X_3^+(2)$ in a structure with mode $X_3^+(1)$ frozen with amplitude of 1.0 bohr. For comparison, the equivalent curve for a pure $X_3^+(2)$ distortion is also shown. (b) Energy contour map for mixed distortions involving nonzero amplitudes of the two unstable X_3^+ normal modes. The oblique position of the absolute minima are caused by very strong anharmonic coupling terms between the two modes.

the basis of eigenvectors of the *ab initio* calculated static normal modes of this symmetry as (0.69, 0.70, 0.07, 0.12, 0.00, −0.01, 0.02, 0.03), where the components are ordered from lower to higher stiffness. One can see that the two lower modes, the only two with negative stiffness, are responsible for the final distortion with essentially equal weight. The contributions of the other modes are basically zero within the estimated accuracy (both of the calculation and of the experimental data) except for a small contribution of the fourth mode. An analogous decomposition of the polarization vector of the E_u experimental polar distortion in

terms of the calculated E_u normal modes yields

$$(0.75, 0.59, 0.06, 0.07, -0.27, 0.06, 0.02, -0.00, 0.02, -0.03, 0.00).$$

Therefore, also in this case, the contribution of the two unstable E_u normal modes is overwhelming.

Hence, neither the experimental structural distortion nor any structure component corresponding to a single irrep can be related to a single unstable normal mode. At least six different normal modes are present with similar weights in the experimental structural distortion. It is especially remarkable that the approximate rigidity of the BiO_6 octahedra, which is observed in the experimental distortion, is achieved through the linear combination of two normal modes of the same symmetry, both involving strongly distorting modes for the octahedra. Their anharmonic coupling is such that it yields an absolute energy minimum where both modes participate in the right proportions to maintain the octahedra approximately rigid. Figure 6 shows the strong magnitude of this anharmonicity. Couplings of types $Q_1^3Q_2$, $Q_1Q_2^3$, and $Q_1^2Q_2^2$ between the amplitudes Q_1 and Q_2 of the normal modes $X_3^+(1)$ and $X_3^+(2)$ displace the energy minimum to a point along the approximate direction (1,1) in the plane $[Q_{X_3^+}(1), Q_{X_3^+}(2)]$, and this linear combination of the two normal modes maintains the TiO_6 octahedra approximately undeformed. In other words, in contrast to what is assumed for the so-called RUMs in framework structures,[33] here the octahedra are approximately rigid in the frozen distortion through anharmonic couplings of octahedra-distorting harmonic normal modes.

Something similar happens with the two unstable polar E_u modes. However, in this case, it is important to note that although their anharmonic coupling yields the right combination to keep the octahedra approximately rigid, this coupling, in contrast to the X_3^+ modes, is very weak. Figure 7 shows that the energy cost of changing the relative signs of the two modes is very small (about 0.5 mRy/f.u.) compared to the depth of 31 mRy of the absolute minimum for the "right" combination of the two E_u modes (see Fig. 5). This implies, as shown in Fig. 7(b), that there are two metastable deep minima for the combination of the two E_u normal modes with opposite signs, in spite of the fact that this would correspond to a structural distortion with significant deformation of the TiO_6 octahedra. Figure 7 shows that the absolute and relative minima are separated by a rather small energy barrier. One can therefore speculate about the possibility of a two-step process for the polarization switching in these materials. The total spontaneous polarization of the system in the ferroelectric phase is necessarily the result of adding the contributions of the two E_u modes, which are of the same order of magnitude. As the energy barrier between the two configurations is small, a minimal opposing field could then be enough for favoring the configuration with the two modes aligned in opposite directions, drastically reducing the polarization. In the second step, the dominant most unstable mode would then change sign overcoming a much higher barrier. The switching properties of BTO, which were considered in the early stages of its investigation as characteristic of a "ferrielectric" material,[34] could be related to this peculiar interplay of these two polar modes.

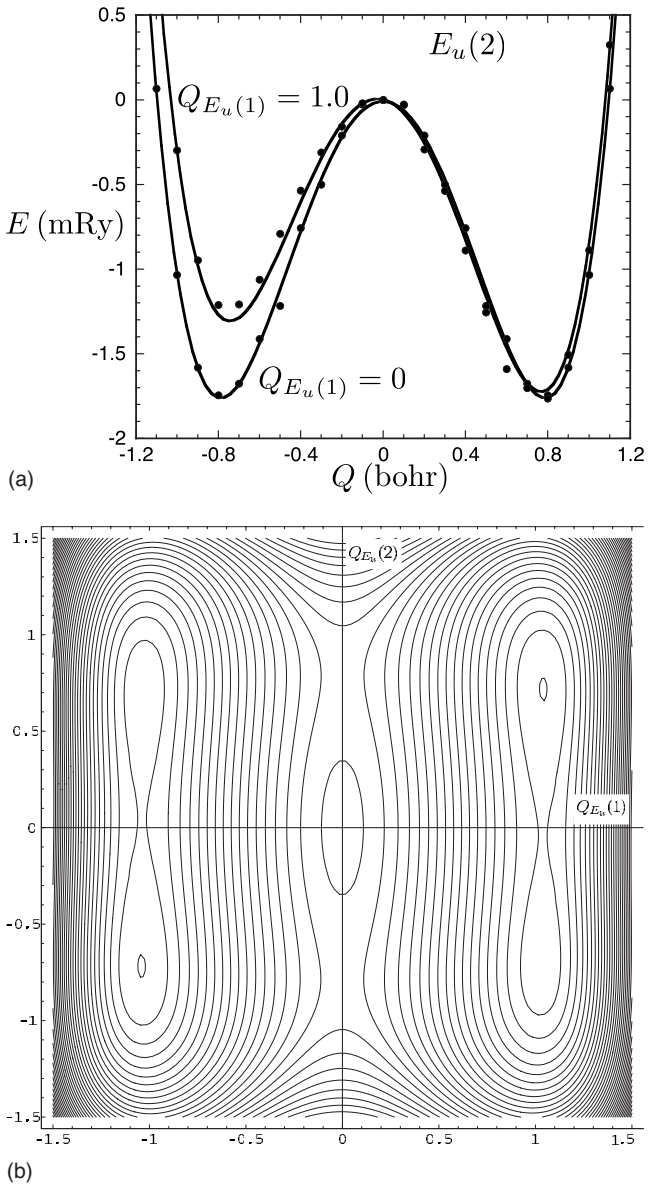

FIG. 7. (a) Relative change of the energy per f.u. as a function of the amplitude of mode $E_u(2)$ in a structure with mode $E_u(1)$ frozen with amplitude of 1.0 bohr. For comparison, the equivalent curve for a pure $E_u(2)$ distortion is also shown. (b) Energy contour map for mixed distortions involving nonzero amplitudes of the two unstable E_u normal modes. The oblique position of the absolute minima are caused by very weak anharmonic coupling terms between the two modes.

VI. SEQUENCE OF PHASE TRANSITIONS OR AN AVALANCHE TRANSITION?

We can now address the question of how the symmetry-breaking $I4/mmm \rightarrow B1a1$ takes place. Although claims of some intermediate phases have been made, including a recent one in Ref. 19, their experimental support is very weak and they contradict other reports with respect to temperature

ranges. Up to now, there is only clear evidence for a single phase transition at about 675 °C. This transition is connected with a strong peak in the dielectric constant, suggesting that the ferroelectric distortion associated with the E_u modes condensates at this point. This is in agreement with our calculations, which find that the polar instability is the strongest one, in contrast to the case of SBT, where the most unstable mode is at the Brillouin zone boundary and yields an intermediate paraelectric orthorhombic phase. If a sequence of phase transitions associated with the different active irreps were to occur in BTO, the expected symmetry changes as temperature is decreased would be $I4/mmm \rightarrow F2mm \rightarrow B2cb \rightarrow B1a1$, with two intermediate phases and a successive spontaneous freezing of distortions of E_u, X_3^+, and X_2^+ symmetries, so that the system would be ferroelectric in all phases except the tetragonal one. These intermediate phases have not been detected up to now. As stressed in the Introduction, the simultaneous condensation of three different order parameters of different symmetries in a single phase transition is an unusual phenomenon even if the transition is discontinuous. There are only a few reported cases of the simultaneous condensation of two primary modes. The phenomenon has been explained through a so-called triggering mechanism,[12] which requires, in general, an unusual negative biquadratic coupling of the order parameters in the Landau potential governing the phenomenology of the system around the transition.[17] The condensation of one of the order parameters can then decrease the effective quadratic stiffness of the second one, and the jump of the first order parameter at the discontinuous transition can be sufficient to make the second one unstable at the same temperature.

In general, a generalized Landau-type explanation requires anharmonic couplings of the order parameters, which favor their simultaneous presence in the structure. We have therefore explored the energy landscape for all active modes mentioned above and determined the couplings among them. The effective biquadratic couplings between pairs of modes are found to be positive in all cases, i.e., modes do not cooperate in the energy minimization and the freezing of one of them positively renormalizes the stiffness coefficients of the others. Figure 8 shows the example of the coupling between the ferroelectric mode $E_u(1)$ depicted in Fig. 4(a) and the mode X_2^+, which is responsible for the symmetry breaking from the orthorhombic $B2cb$ to the monoclinic $B1a1$ symmetry. The X_2^+ mode introduces correlated rigid rotations of the central octahedra in the perovskite slabs around the z tetragonal axis, which are achieved by atomic displacements of the O_1 atoms (see Fig. 1). As can be seen in Fig. 8, this distortion mode is quite effective in reducing the energy, almost as much as the most unstable polar mode $E_u(1)$. However, the presence of the latter drastically reduces the depth of its energy well as a result of the strong positive biquadratic coupling between the two modes. Hence, their simultaneous condensation in the structure is penalized. We observe a similar type of interplay between all pairs of unstable normal modes. The effect of the coupling of the two most unstable modes, $E_u(1)$ and $X_3^+(1)$, is depicted in Fig. 9. The presence of the $X_3^+(1)$ normal mode (with an amplitude corresponding to the minimum of its energy curve) drastically

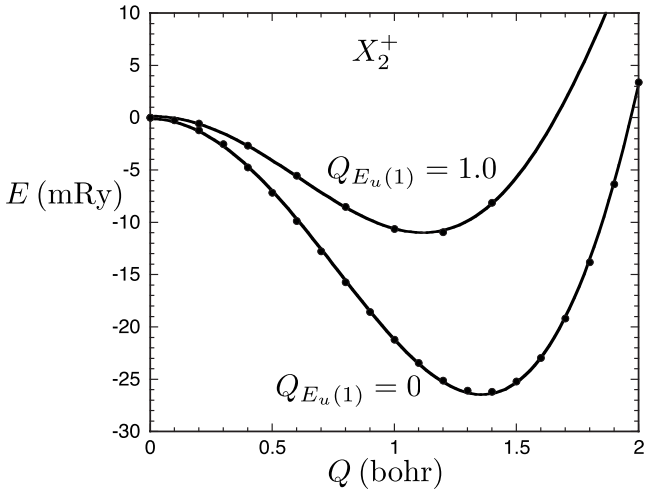

FIG. 8. Relative energy change per f.u. as a function of the amplitude of the unstable mode of symmetry X_2^+, which is responsible for the monoclinic ground state of BTO. The lower points corresponds to this mode as a single distortion, while the higher points are obtained when mode $E_u(1)$ at a fixed amplitude corresponding to its energy minimum is superposed. The curves correspond to fitted 2-4-6 polynomials.

reduces the energy decrease achieved with the $E_u(1)$ distortion. The effect is, however, not as strong as in SBT, where the presence of one of the two competing modes fully stabilized the other one.[10]

On the other hand, trilinear couplings between three of the modes would favor a triggering mechanism independently of the sign of the coupling. However, our investigation of these types of couplings shows that they are too weak to prevail over the unfavorable quadratic couplings. This can be already seen from the weak variation in the amplitude of the modes in the global mixed minimum with respect to their amplitudes at the energy minimum when each mode is considered separately.

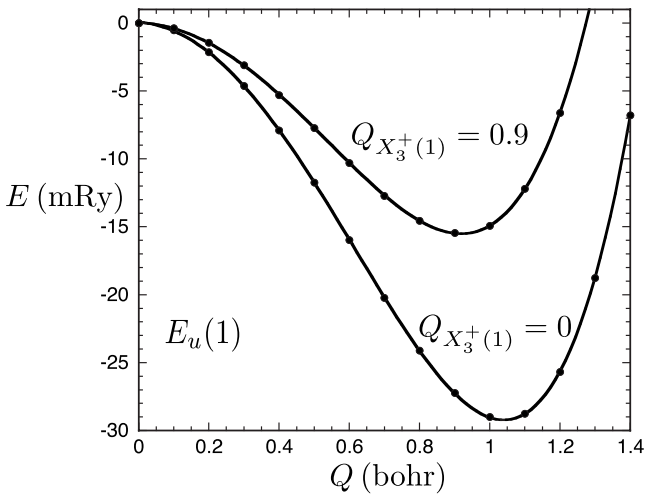

FIG. 9. Relative change of the energy per f.u. as a function of the amplitude of mode $E_u(1)$ in a structure with mode X_3^+ frozen with amplitude of 0.9 bohr. For comparison, the equivalent curve for a pure $E_u(1)$ distortion is also shown.

Obviously, the anharmonic couplings relevant in the effective Landau free energy may considerably differ from those of the underlying energy map as they are, in general, temperature dependent. We cannot rule out the possibility that thermal effects are so strong as to change the sign of these anharmonic interactions and thus drastically affect the interplay between the modes. However, we consider this quite unlikely. The present study shows that there is no clear feature in the energy landscape that favors the simultaneous condensation of the three primary symmetry-breaking modes present in the ground state of the system. One can only state that the anharmonic couplings that play against this phenomenon are significantly weaker than in SBT. Therefore, the apparent absence of intermediate phases in BTO remains to be explained. In any case, one should not forget that it can be very difficult to discern as distinct close consecutive phase transitions at high temperatures. Even at low temperatures, it can become a challenge to resolve a sequence of transitions within a small temperature range (see, for example, the work reported in Ref. 35).

VII. CONCLUSIONS

A complex interplay between different structural instabilities including the ferroelectric one is characteristic for the whole Aurivillius family, and only the combined symmetry-breaking effects of several unstable modes can explain the observed ferroelectric-phase symmetries. In some Aurivillius compounds such as $Sr_2BiTa_2O_9$, this leads to a sequence of thermal phase transitions, as expected from the Landau theory. However, in some other compounds, the different order parameters present in the ferroelectric phase seem to condense simultaneously. Instead of the expected sequence of phase transitions (one for each primary order parameter), a single phase transition has been observed. We denote this peculiar behavior as an avalanche phase transition, i.e., a single phase transition whose symmetry break requires several order parameters. According to the literature, BTO is one of the Aurivillius compounds where an avalanche transition exists. Our first-principles energy and phonon calculations of this compound and their quantitative comparison with experimental data evidence a complex interplay of six different normal modes for the stabilization of the distorted ferroelectric phase. As claimed in a single-crystal diffraction study, and in contrast to powder diffraction results, BTO is confirmed to be monoclinic due to a strong unstable mode that breaks the orthorhombic symmetry. This additional primary instability involves only rotations around z of the TiO_6 octahedra in the central layer of the perovskite slabs and appears, in addition to the polar and tilting modes, responsible for the orthorhombic distortion, which are the only ones present in other orthorhombic compounds.

The normal-mode analysis of the energy landscape around the tetragonal phase shows a rather complex relation between the static structure of BTO and the corresponding harmonic normal modes. Both the instabilities at the X point of the Brillouin zone and the polar ones split into pairs of unstable modes leading to a total of at least six different normal modes with significant and comparable weight in the experimental distortion. The observed approximate rigidity of the BiO_6 octahedra is in fact achieved through the linear combination of two normal modes of the same symmetry that would strongly distort the octahedra if considered separately. Thus, in contrast to the usual picture, the octahedra are rigid only through anharmonic couplings and not within the harmonic approximation.

Our study of the energy landscape associated with the calculated unstable modes failed to show any feature that would favor the simultaneous condensation of the different order parameters. This makes it quite unlikely that a triggering mechanism is behind the existence of a single avalanche phase transition. Therefore, the apparent absence of intermediate phases in BTO remains to be explained. Given the experimental difficulties intrinsic to high-temperature investigations and the limitations of the powder method for diffraction analysis (the only method used up to now at high temperatures), it cannot be ruled out that the intermediate phases indeed exist but remain to be detected by more accurate experimental techniques. Each of these intermediate transitions should nevertheless exhibit the joint condensation of two modes of the same symmetry, thus placing $Bi_4Ti_3O_{12}$ outside the standard soft-mode paradigm.

ACKNOWLEDGMENTS

We thank R. Withers for illuminating discussions. This work was supported by the Spanish Ministry of Education and Science (Project No. MAT 2005-05216) and the Basque Government (Project No. IT-282-07). Part of the computer time was provided by the SGI/IZO-SGIker at the UPV/EHU (supported by the Spanish Ministry of Education and Science and the European Social Fund).

APPENDIX: THE BOND-VALENCE GLOBAL INSTABILITY INDEX

When studying the low-energy landscape around the tetragonal configuration of the Aurivillius compound SBT,[10] it was observed that a magnitude computed within the empirical bond-valence method[36] strikingly mimicked the behavior of the *ab initio* total energy. This magnitude is the square of the so-called global instability index Gii,[37] which measures the average deviation of the apparent atomic valences (calculated through the bond-valence method) from their nominal values. The Gii^2 and energy maps could be approximately related through a single scale factor of 500 mRy per square valence unit.[24] Here, we present a similar comparison for some of the critical modes of $Bi_4Ti_3O_{12}$ discussed above.

According to the bond-valence formalism, the apparent (V_i) valence of an atom is obtained by means of bond-valence sums that depend on the distances of the surrounding counterions and empirical parameters:[36]

$$V_i = \sum_j v_{ij}, \quad v_{ij} = \exp\left(\frac{d_{ij} - R_{ij}}{b}\right),$$

where R_{ij} are the bond lengths, d_{ij} are parameters that depend on the kinds of bonded atoms, and $b=0.37$ Å is a universal constant. The global instability index is defined as the root

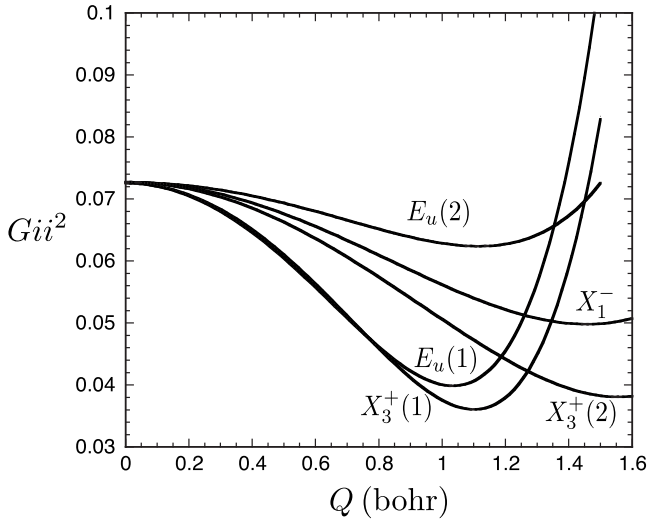

FIG. 10. Square of global instability index Gii^2 as a function of the amplitude of unstable static normal modes, to be compared to the energy behavior shown in Fig. 5.

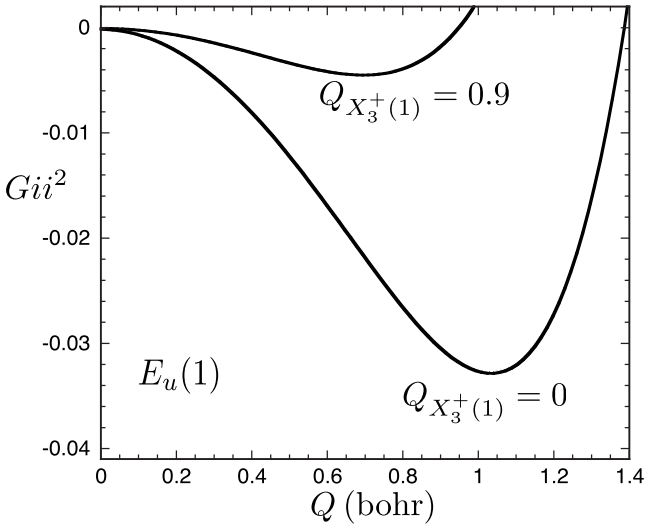

FIG. 11. Relative change of the square of global instability index Gii^2 as a function of the amplitude of the normal mode $E_u(1)$ in a structure with normal mode $X_3^+(1)$ frozen with amplitude of 0.9 bohr. For comparison, the equivalent curve for a pure $E_u(1)$ distortion is also shown. The corresponding figure for the energy picture is shown in Fig. 9.

mean square over all the atoms of the difference between their apparent (V_i) and nominal (V_i^0) valences:

$$Gii^2 = \frac{1}{N}\sum_{i=1}^{N} (V_i - V_i^0)^2,$$

where N is the number of atoms per unit cell. For the calculations of the apparent valences, we have used $d_{\text{Bi-O}} = 2.094$ Å, $d_{\text{Ti-O}} = 1.815$ Å, and $d_{\text{O-O}} = 1.500$ Å, and the cutoff for the interatomic distances was set to 4.5 Å.

Figure 10 shows the Gii^2 curves for distortions corresponding to the unstable modes of symmetries E_u, X_3^+, and X_1^-, which can be directly compared to the corresponding *ab initio* energy maps of Fig. 5. The similarity between the figures is remarkable, but it is not so strong as in SBT. The transformation factor relating the scales employed in the two figures is about 700 mRy per square valence unit. The normal mode $X_3^+(1)$ is more unstable than the $E_u(1)$, while in the energy maps, it is the reverse. Also, the minima of the Gii^2 curves for the $X_3^+(2)$ and X_1^- distortions are significantly shifted to larger values.

Despite these differences, Gii^2 qualitatively behaves as the energy, and this property is also observed when coupling effects between these critical modes are considered. The effect of the coupling between the normal modes $E_u(1)$ and $X_3^+(1)$ from the point of view of the global instability index can be seen in Fig. 11. The presence of the $X_3^+(1)$ distortion reduces the instability of the $E_u(1)$ distortion in a similar way as in the energy calculation shown in Fig. 9. The factor relating the scales of both figures is the same as the one between Figs. 5 and 10. For other couplings, the agreement is maintained at a similar qualitative level. In particular, the signs of the couplings discussed in the previous section are already seen on the behavior of the global instability index.

As pointed out in Ref. 24, it should be stressed that the parallelism between energy and the Gii^2 is limited to the low-energy unstable normal modes. This means that these modes, which are favorable for the minimization of the system energy, cannot, in general, be derived from empirical arguments by considering only the optimization of the *Gii* index.

*jm.perez-mato@ehu.es

[1] D. Vanderbilt, Curr. Opin. Solid State Mater. Sci. **2**, 701 (1997).
[2] R. Resta, Modell. Simul. Mater. Sci. Eng. **11**, R69 (2003).
[3] *Physics of Ferroelectrics: A Modern Perspective*, Topics in Applied Physics, edited by K. Rabe, Ch. H. Ahn, and J. M. Triscone (Springer-Verlag, Berlin, 2007).
[4] A. Bruce, Adv. Phys. **29**, 111 (1980).
[5] W. Zhong and D. Vanderbilt, Phys. Rev. Lett. **74**, 2587 (1995).
[6] A. D. Rae, J. G. Thompson and R. L. Withers, Acta Crystallogr., Sect. B: Struct. Sci. **48**, 418 (1992).
[7] A. D. Rae, J. G. Thompson, R. L. Withers, and A. C. Willis, Acta Crystallogr., Sect. B: Struct. Sci. **46**, 474 (1990).
[8] R. Macquart, B. J. Kennedy, B. A. Hunter, and C. J. Howard, J. Phys.: Condens. Matter **14**, 7955 (2002).
[9] R. Macquart, B. Kennedy, T. Vogt, and C. J. Howard, Phys. Rev. B **66**, 212102 (2002).
[10] J. M. Perez-Mato, M. Aroyo, A. Garcia, P. Blaha, K. Schwarz, J. Schweifer, and K. Parlinski, Phys. Rev. B **70**, 214111 (2004).

[11] L. D. Landau and E. M. Lifshitz, *Statistical Physics* (Pergamon, Oxford 1959).
[12] J. C. Toledano and P. Toledano, *Landau Theory of Phase Transitions* (World Scientific, Singapore 1987).
[13] A. Onodera, T. Kubo, K. Yoshio, S. Kojima, H. Yamashita, and T. Takama, Jpn. J. Appl. Phys., Part 1 **39**, 5711 (2000).
[14] C. H. Hervoches, J. T. S. Irvine, and P. Lightfoot, Phys. Rev. B **64**, 100102(R) (2001).
[15] J. S. Kim, C. I. Cheon, H. S. Shim, and C. H. Lee, J. Eur. Ceram. Soc. **21**, 1295 (2001).
[16] A. Snedden, C. H. Hervoches, and P. Lightfoot, Phys. Rev. B **67**, 092102 (2003).
[17] J. Holakovsky, Phys. Status Solidi B **56**, 615 (1973).
[18] Yu. M. Gufan and E. S. Larin, Sov. Phys. Solid State **22**, 270 (1980).
[19] Q. Zhou, B. J. Kennedy, and C. J. Howard, Chem. Mater. **2003**, 50025 (2003).
[20] R. Machado, M. G. Stachiotti, R. L. Migoni, and A. H. Tera, Phys. Rev. B **70**, 214112 (2004).
[21] P. Blaha, K. Schwarz, G. Madsen, D. Kvasnicka, and J. Luitz, WIEN2K, an augmented plane wave+local orbitals program for calculating crystal properties, Karlheinz Schwarz, Technische Universitt Wien, Austria, 2001.
[22] J. P. Perdew, K. Burke, and M. Ernzerhof, Phys. Rev. Lett. **77**, 3865 (1996).
[23] K. Parlinski, PHONON Software, Cracow, 2002.
[24] I. Etxebarria, J. M. Perez-Mato, A. Garcia, P. Blaha, K. Schwarz, and J. Rodriguez-Carvajal, Phys. Rev. B **72**, 174108 (2005).
[25] C. Hervoches and P. Lightfoot, Chem. Mater. **11**, 3359 (1999).
[26] S. E. Cummins and L. E. Cross, J. Appl. Phys. **39**, 2268 (1968).
[27] *International Tables for Crystallography, Volume A: Space Group Symmetry*, 5th ed., edited by T. Hahn (Kluwer, Dordrecht, 2002).
[28] M. I. Aroyo, A. Kirov, C. Capillas, J. M. Perez-Mato, and H. Wondratschek, Acta Crystallogr., Sect. A: Found. Crystallogr. **62**, 115 (2006).
[29] M. I. Aroyo, J. M. Perez-Mato, C. Capillas, E. Kroumova, S. Ivantchev, G. Madariaga, A. Kirov, and H. Wondratschek, Z. Kristallogr. **221**, 15 (2006).
[30] For the E_u, polar modes, this fact was already pointed out in Ref. 20. The present calculations show that a similar situation happens for the other dominant distortion of X_3^+, symmetry.
[31] Y. E. Kitaev, M. I. Aroyo, and J. M. Perez-Mato, Phys. Rev. B **75**, 064110 (2007).
[32] D. Nuzhnyy, S. Kamba, P. Kuzel, S. Veljko, V. Bovtun, M. Savinov, J. Petzelt, H. Amorin, M. E. V. Costa, A. L. Kholkin, Ph. Boullay, and M. Adamczyk, Phys. Rev. B **74**, 134105 (2006).
[33] A. P. Giddy, M. T. Dove, G. S. Pawley, and V. Heine, Acta Crystallogr., Sect. A: Found. Crystallogr. **49**, 697 (1993).
[34] D. L. Hamilton, J. Appl. Phys. **38**, 10 (1967).
[35] Y. Fuji, S. Hoshino, Y. Yamada, and G. Shirane, Phys. Rev. B **9**, 4549 (1974).
[36] I. D. Brown, Acta Crystallogr., Sect. B: Struct. Sci. **48**, 553 (1992).
[37] A. Salinas-Sanchez, J. L. Garcia-Muñoz, J. Rodriguez-Carvajal, R. Sanchez-Puche, and J. L. Martinez, J. Solid State Chem. **151**, 245 (1992).
[38] Preliminary results of this work were presented at the International Conference on Density Functional Theory and Transmission Electron Microscopy (DFTEM), Vienna, Austria, 2006.
[39] To maintain the notation of previous literature, we do not use the new official space group labels introduced in the latest edition of the International Tables for Crystallography (Ref. 27), where *B*2*cb* becomes *B*2*eb*, *Bmab* is *Bmeb*, etc.
[40] The program AMPLIMODES recently added to the Bilbao Crystallographic Server (www.cryst.ehu.es) (Refs. 28 and 29) can be used to automatically do this calculation for any distorted structure.